Radiation Resistance of Duplex Stainless Steel under Proton Irradiation : Correlation between Microstructural Evolution and Nano-mechanical Properties

Date : May 22nd, 2025
Time : 15:30 ~ 15:50

Hyun Joon Eom, Sumin Kim, Chaewon Jeong,
Ye-jin Kweon, Changheui Jang* (KAIST), Chaewon Kim (KAERI)

Nuclear & High Temperature Materials Laboratory
Department of Nuclear & Quantum Engineering, KAIST

Contents

Introduction

[1] J.H Shin et. al., Journal of Nuclear Materials, 564:153678~ (2022)
[2] B.S Kong et. Al., Journal of Nuclear Materials, 533:152656~ (2021)

❑ Duplex Stainless Steel in Various Nuclear Reactors

- **Excellent Corrosion Resistance & Mechanical Properties**
  - Duplex structure : Ferritic + Austenitic phases
  - Widely used in nuclear reactor components (e.g. cladding materials)
- **Microstructural Evolution of Matrices under irradiation condition**
  - Austenitic : Void swelling → Mechanical Degradation
  - Ferritic : Spinodal Decomposition → Embrittlement
  - Cladding tube : Requirement of thin-wall structure due to neutron penalty

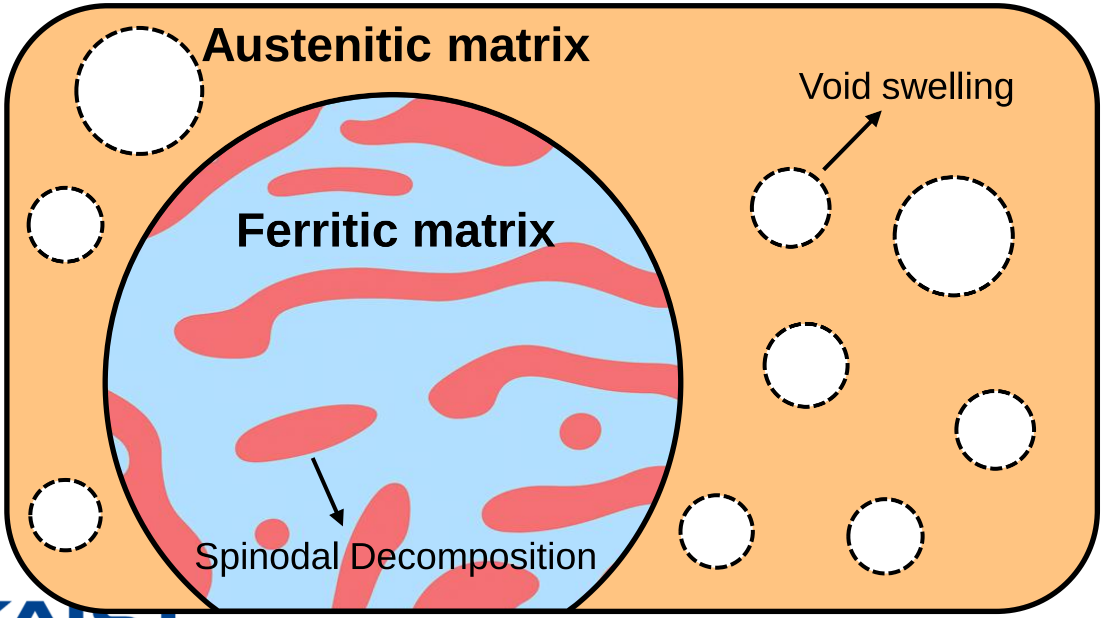

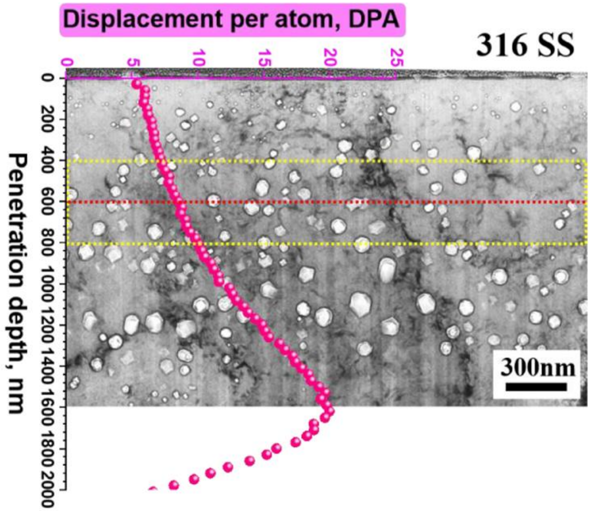

▲ TEM image of void swelling in commercial austenitic stainless steel after heavy ion irradiation (316 SS) [1]

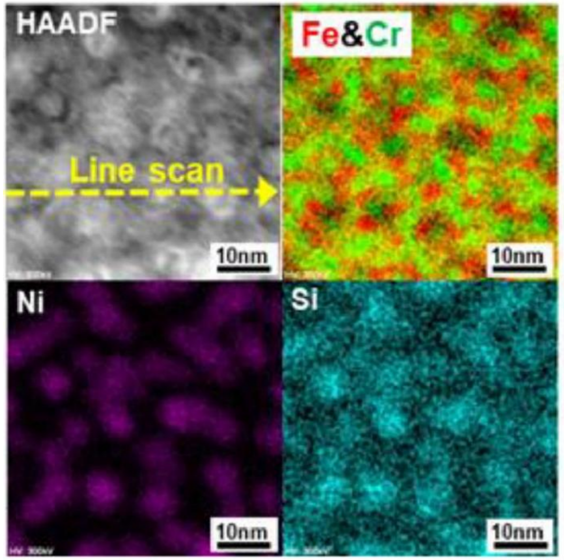

▲ TEM image and corresponding EDS mapping data for showing the presence of spinodal decomposition in δ-ferrite after proton irradiation [2]

Introduction

[1] H. Kim et. al., Journal of Nuclear Materials, 507:1~14 (2018)

❑ Development of Alumina-forming duplex stainless steel (ADSS)

- **Chemical composition**
  - 18 – 21 Ni & 16 – 21 Cr
    - ◻ Ni : Austenitic stabilizer & High-temperature tensile strength
    - ◻ Cr : Ferritic stabilizer & Oxidation resistance
  - 5 – 6 Al
    - ◻ Formation of **B2-NiAl precipitates** in both austenitic & ferritic matrix

Composition (wt.%)	Fe	Cr	Ni	Al	Nb	Mn	Si	C
ADSS	Bal.	16.76	19.2	5.84	0.33	0.84	0.11	0.0874
APM (Ref.)	Bal.	21.9	-	5.81	-	0.16	0.28	0.03
310 SS (Ref.)	Bal.	24.7	19	-	-	0.87	0.06	0.06

▲ Chemical composition of the ADSS and other commercial Fe-base reference alloys (APM, 310 SS) measured by ICP-AES analysis [1]

- **Role of B2-NiAl precipitates in ADSS**
  - Better mechanical properties compared to the other alloys (APM : Ferritic, 310 SS : Austenitic)
  - Better corrosion resistance in oxidation & MSR environments
    - ◻ Dissolution of B2-NiAl near surface (B2-denude zone) → Al reservoir for the formation of α-alumina (protective layer)
  - Better radiation resistance for both matrices?

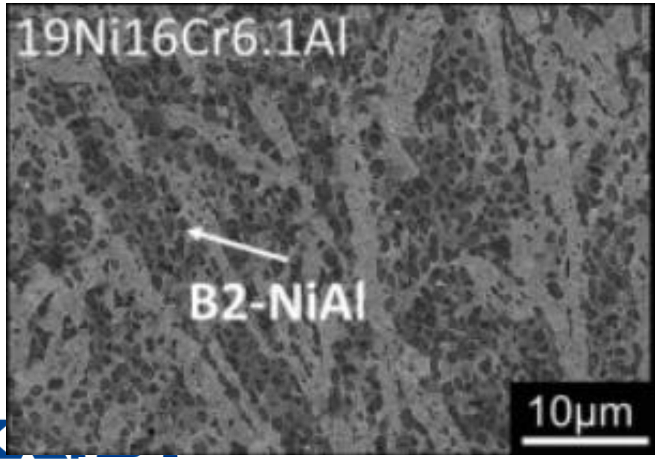

▲ SEM image of ADSS with B2-NiAl precipitates [1]

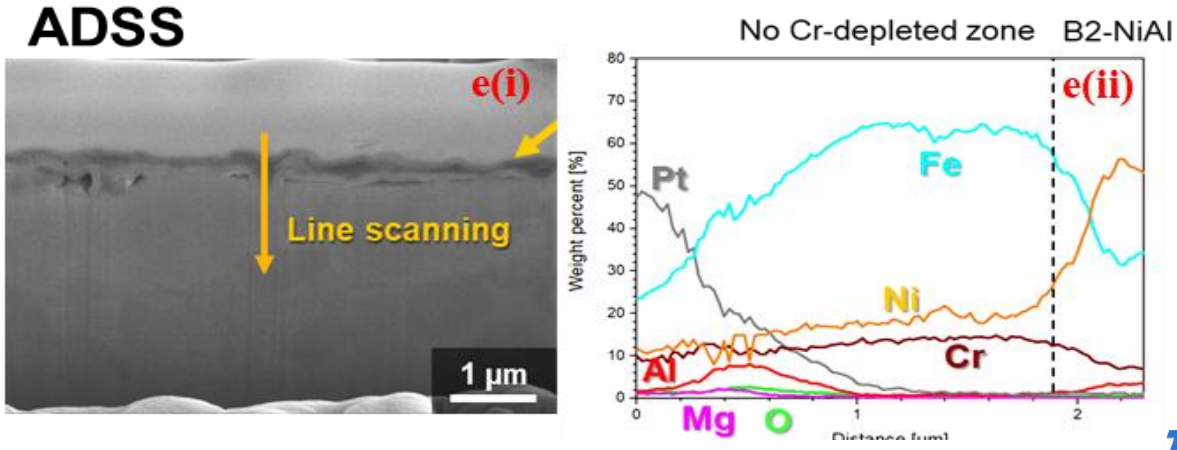

▲ Cross-sectional SEM image of ADSS after corrosion test

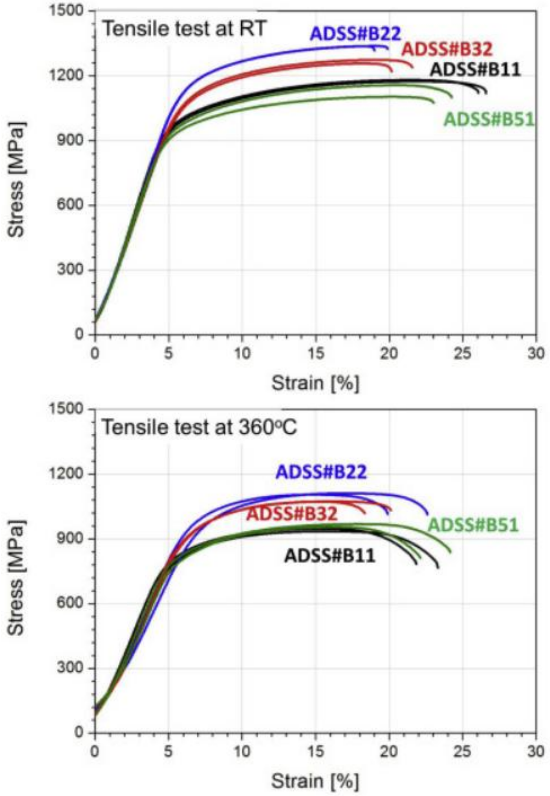

▲ Tensile test results for various ADSS alloys [1]

Experimental Approach : Proton Irradiation & Microstructural Analysis

❑ Proton Irradiation for simulation of neutron irradiation

- **Materials**
  - **ADSS : Comparison between Austenitic matrix and Ferritic matrix**

- **Irradiation condition**
  - **Stopping and Range of Ions in Matter (SRIM) simulation**
    - ◻ 360 ℃ static defocusing beam with 2 MeV proton in Michigan Ion Beam Laboratory (MIBL)
    - ◻ 40 eV displacement energy in Kinchin-Pease model (K-P model)
    - ◻ Targeted damage : 1 ~ 2 dpa below 1 μm depth region
    - ◻ Dose rate : 1×10^{-5} dpa /sec

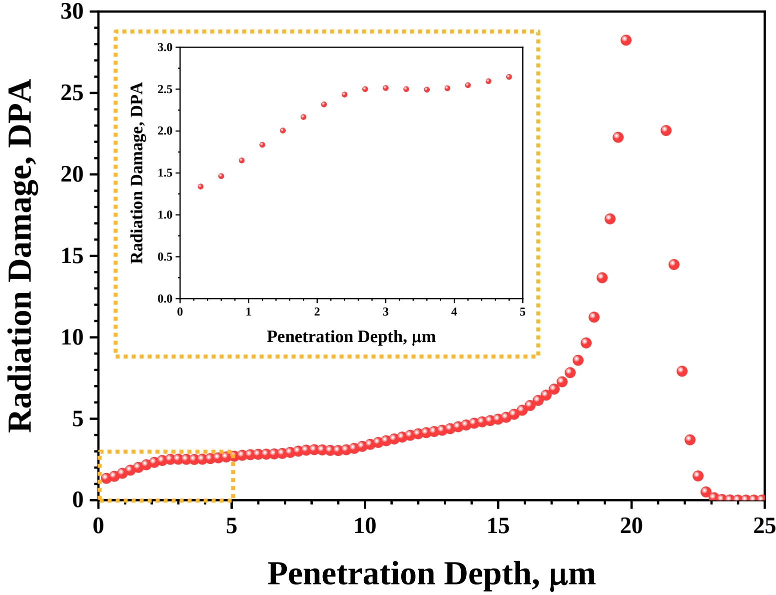

▲ The radiation damage (DPA) as a function of penetration depth (μm) in SRIM code simulation

❑ Microstructural Analysis

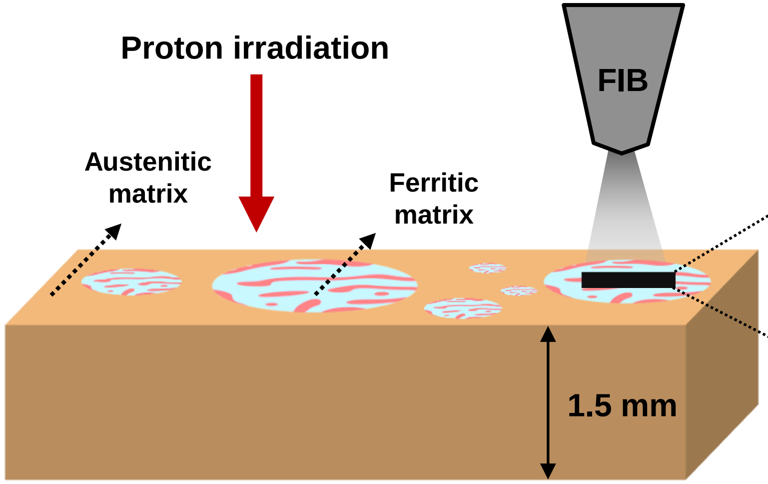

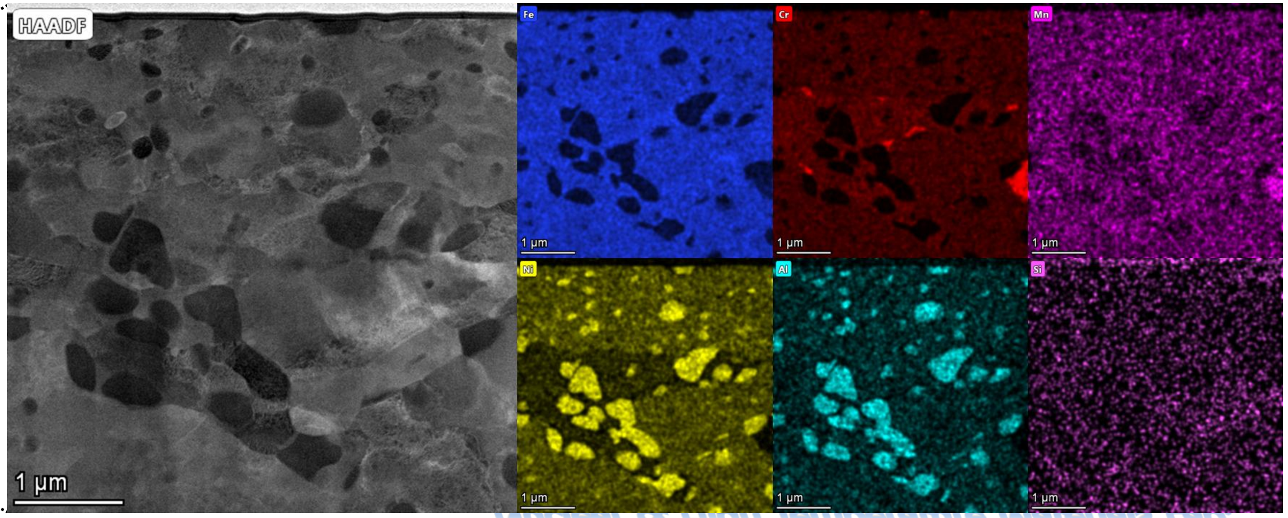

▲ Graphical schematic for TEM specimen fabrication from unirradiated / irradiated ADSS alloys via FIB

Experimental Approach : Nano-indentation

Nano-indentation test for evaluating radiation-induced hardening

- **Nano-indentation test condition**
  - Nano-DMA mode with Berkovich indenter (KAIST NQE)
  - 10 x 10 arrays from unirradiated & irradiated each matrices of ADSS at room temperature

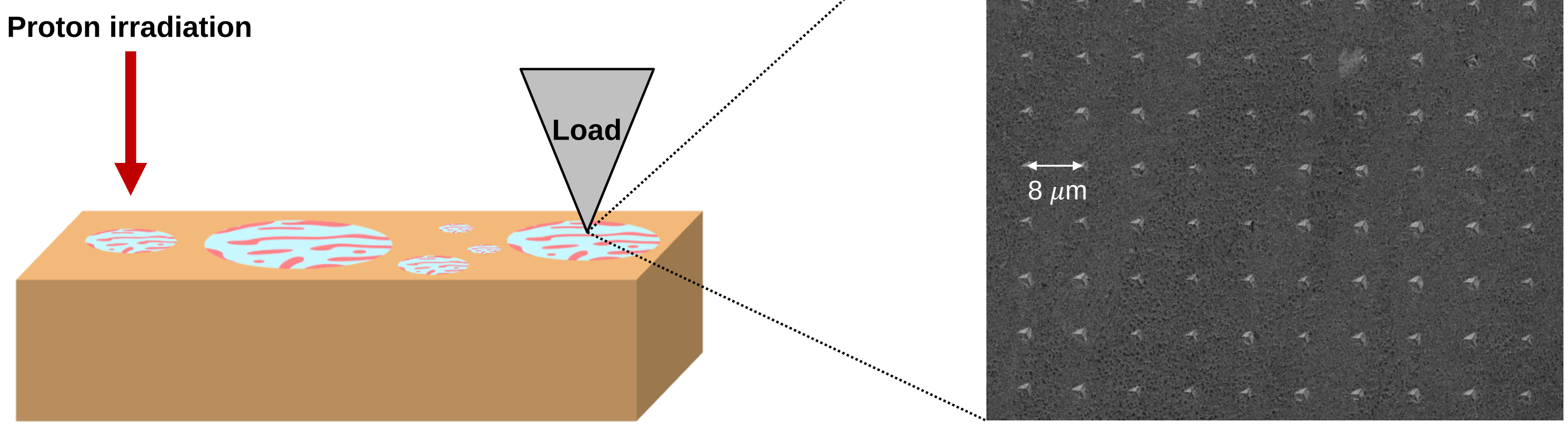

- **Evaluation of Radiation-induced hardening under proton irradiation**
  - Bulk hardness interpretation via **Nix-Gao modelling** from measured nano-hardness
  - Quantifying the radiation hardening as a function of microstructural evolution of each matrix

Results : Microstructural Evolution

❑ Overview Microstructural Evolution within matrices

- **Austenitic matrix before & after irradiation**
  - **Before Irradiation**
    - ◻ Smaller B2-NiAl precipitates compared to ferritic matrix
    - ◻ Smaller number density of B2-NiAl
  - **After Irradiation**
    - ◻ Huge dissolution of large B2-NiAl precipitates
    - ◻ No re-precipitation of B2-NiAl precipitates
    - ◻ Formation of Nb-rich precipitates
- **Ferritic matrix before & after irradiation**
  - **Before Irradiation**
    - ◻ Large B2-NiAl precipitates
    - ◻ High Number density of B2-NiAl
  - **After Irradiation**
    - ◻ Dissolution of large B2-NiAl precipitates
    - ◻ Re-precipitation of smaller size B2-NiAl precipitates nearby

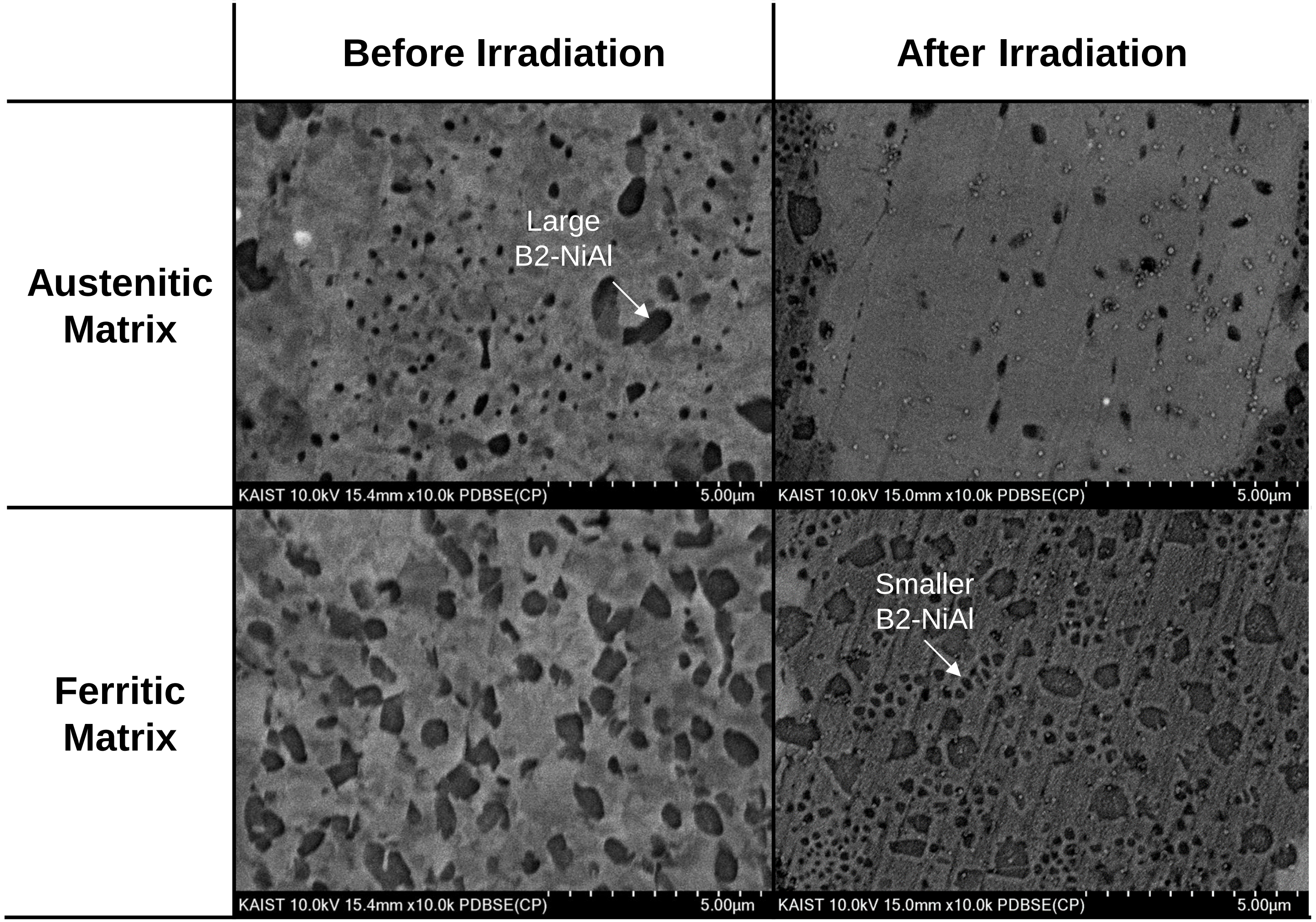

▲ SEM micrographs of microstructural evolution of both austenitic and ferritic matrix in ADSS alloy along the proton irradiation

Results : Microstructural Evolution

- **TEM analysis on microstructural evolution of austenitic matrix**
  - **Formation of γ'-Ni_3Al precipitates**
    - Before Irradiation
      - Uniform Ni & Al distribution **without γ'-Ni_3Al precipitates**
    - After Irradiation
      - **Formation of nano-sized γ'-Ni_3Al precipitates** (Localized Ni & Al enrichment + FFT pattern)
      - Average size (radius) : 4.50 $\pm$ 1.29 nm, Number density : 3.70 $\pm$ 0.28 $\times$ 10^{23} # / m^3

Unirradiated ADSS (Austenitic matrix)

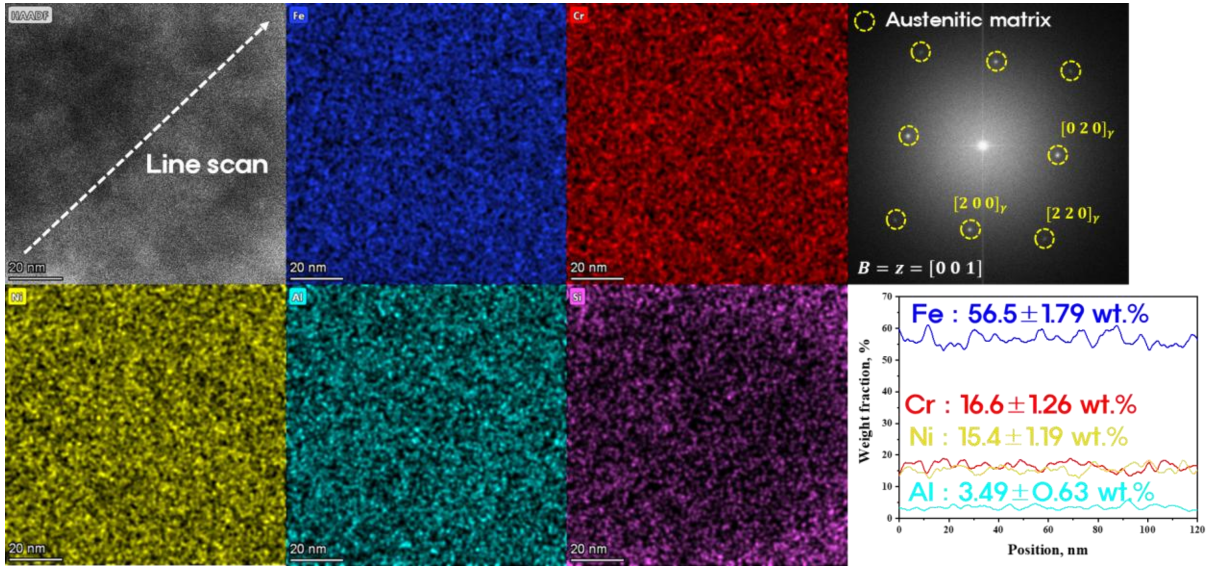

Irradiated ADSS (Austenitic matrix)

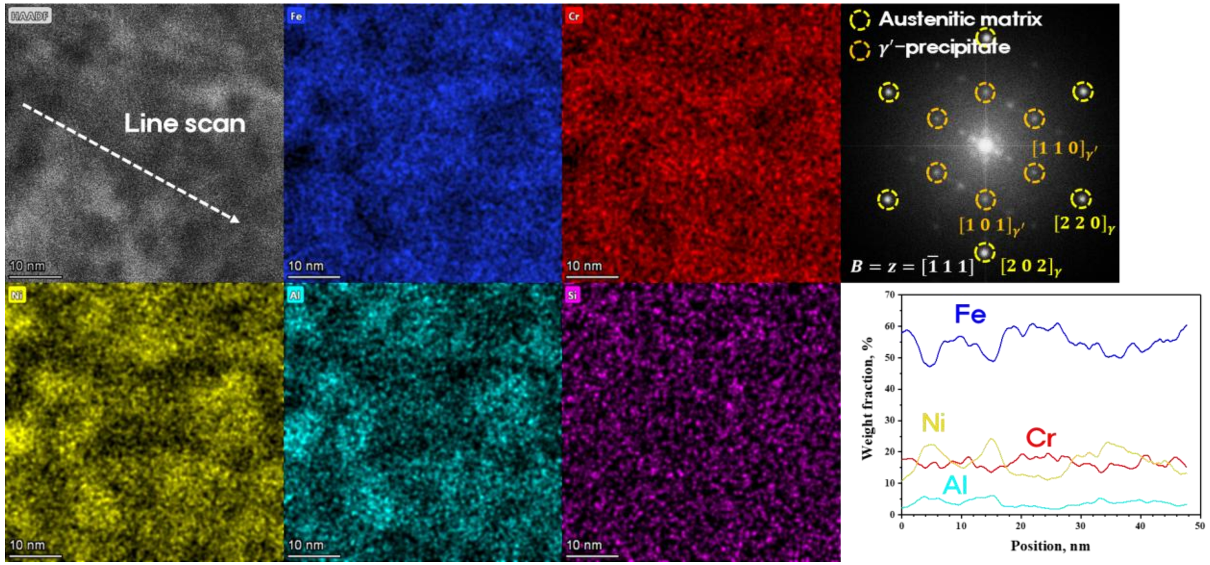

[1] M.A. Moretti, Microstructure and property models of alloy 718 applicable for simulation of manufacturing processes (2022)

❑ TEM analysis on microstructural evolution of austenitic matrix

- **Strengthening effect estimation for γ'-Ni_3Al precipitates in Austenitic matrix**
  - **Shearing Mechanism : Modulus & Coherency Strengthening**
    - ☐ $\Delta\tau_{mod} = 0.0055 \cdot (\Delta G)^{3/2} \cdot \left(\frac{2f}{G}\right)^{1/2} \cdot \left(\frac{D}{2b}\right)^{\frac{3m}{2}-1}$
    - ☐ $\Delta\tau_{coh} = \alpha \cdot G \cdot \varepsilon^{3/2} \cdot \left(\frac{D \cdot f}{b}\right)^{1/2}$
  - **Bypass Mechanism : Orowan Strengthening (Dominant)**
    - ☐ Precipitate radius (~ 4.5 nm) > Critical radius (~ 0.51 nm)
    - ☐ $\Delta\tau_{Orowan} = \frac{0.28 \cdot G \cdot b}{\pi \cdot \lambda_s \cdot (1-\nu)^{0.5}} ln\left(\frac{1.63 \cdot r}{b}\right) \sim 680.42$ MPa

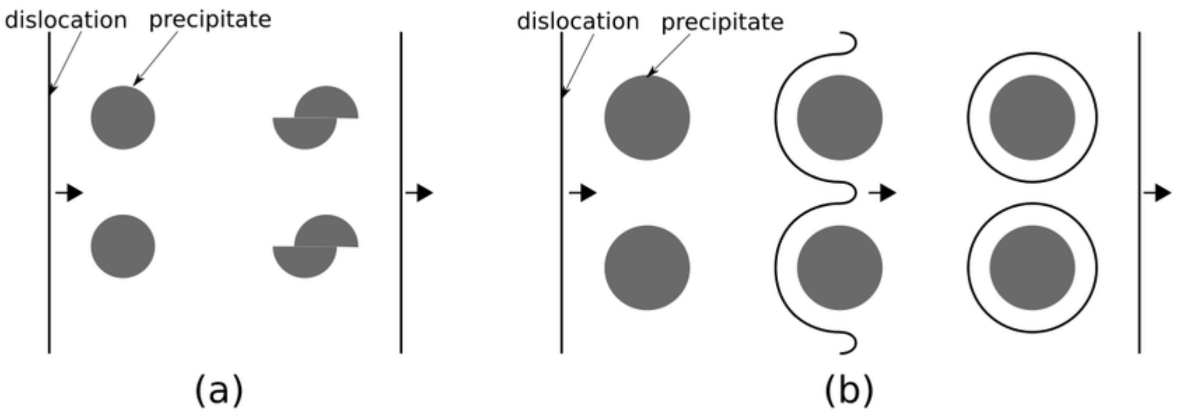

▲ Graphical schematic for precipitate shearing mechanism and bypass mechanism [1]

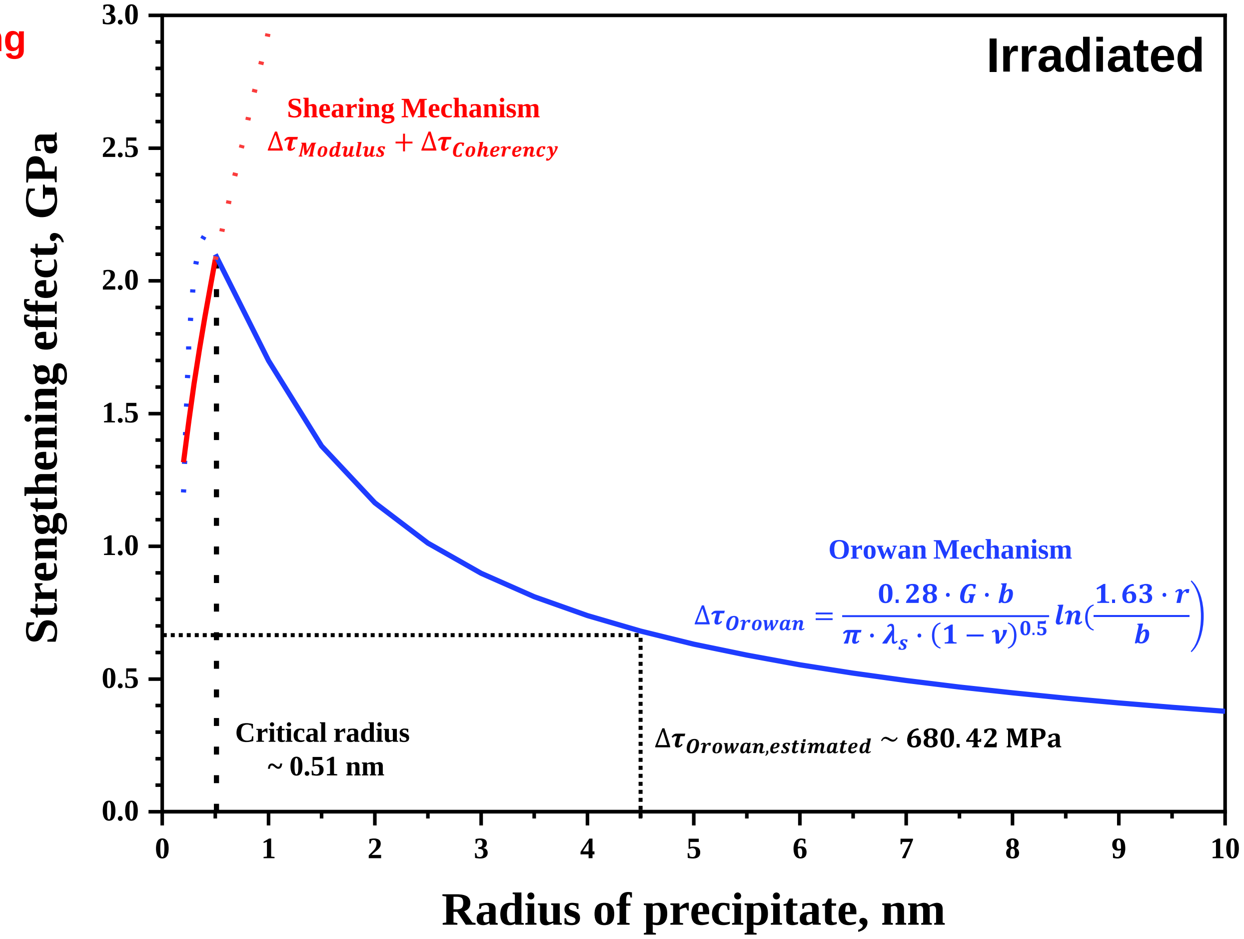

▲ Estimated strengthening effect of γ'-Ni_3Al precipitates as a function of precipitate radius (nm)

Results : Microstructural Evolution

❑ TEM analysis on microstructural evolution of ferritic matrix

- **Coarsening of Nano-sized B2-NiAl in ferritic matrix**
  - **Before Irradiation**
    - ◻ Average size : 9.05 ± 3.67 nm, Number density : 2.4 ± 0.68 × 10^{22} # / m^3
  - **After Irradiation**
    - ◻ **More distinct Ni distribution** in nano-sized B2-NiAl precipitates
    - ◻ Average size : 15.75 ± 3.36 nm, Number density : 9.67 ± 0.43 × 10^{21} # / m^3

Unirradiated ADSS (Ferritic matrix)

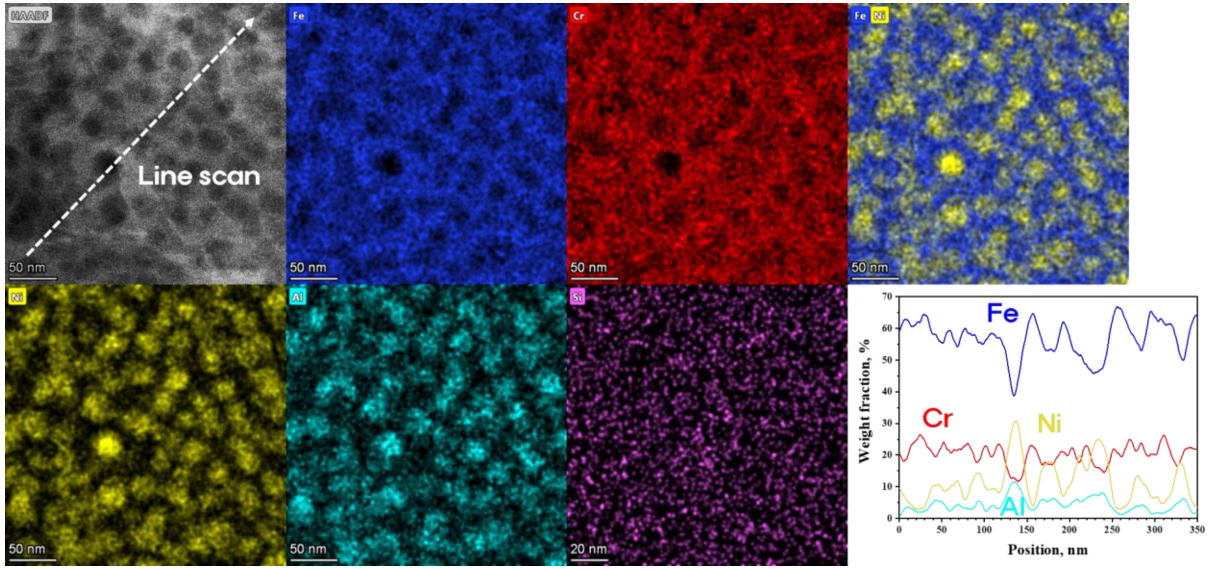

Irradiated ADSS (Ferritic matrix)

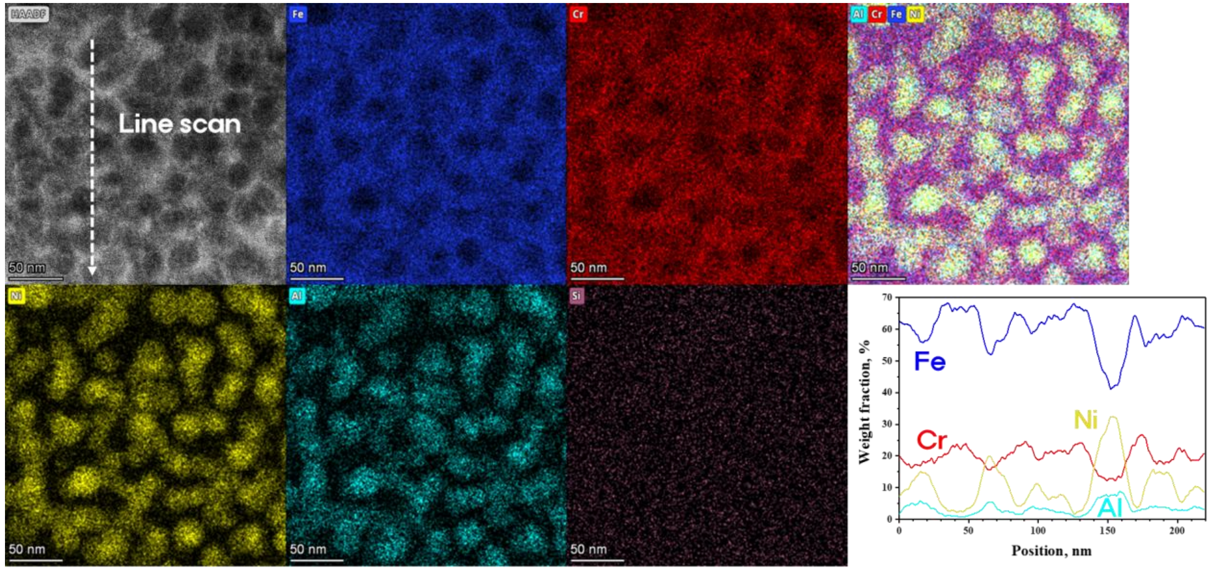

Results : Microstructural Evolution

- **TEM analysis on microstructural evolution of ferritic matrix**
  - **Strengthening effect estimation for coarsened nano-sized B2-NiAl precipitates in ferritic matrix**
    - **Orowan Strengthening (Dominant)**

☐ $\tau_{Orowan,unirr} = \frac{0.28 \cdot G \cdot b}{\pi \cdot \lambda_s \cdot (1-\nu)^{0.5}} ln\left(\frac{1.63 \cdot r}{b}\right)$ ~248.9 MPa vs. $\tau_{Orowan,irr} = \frac{0.28 \cdot G \cdot b}{\pi \cdot \lambda_s \cdot (1-\nu)^{0.5}} ln\left(\frac{1.63 \cdot r}{b}\right)$ ~340.0 MPa : $\Delta\tau_{Orowan,B2} \sim 91.1\ MPa$

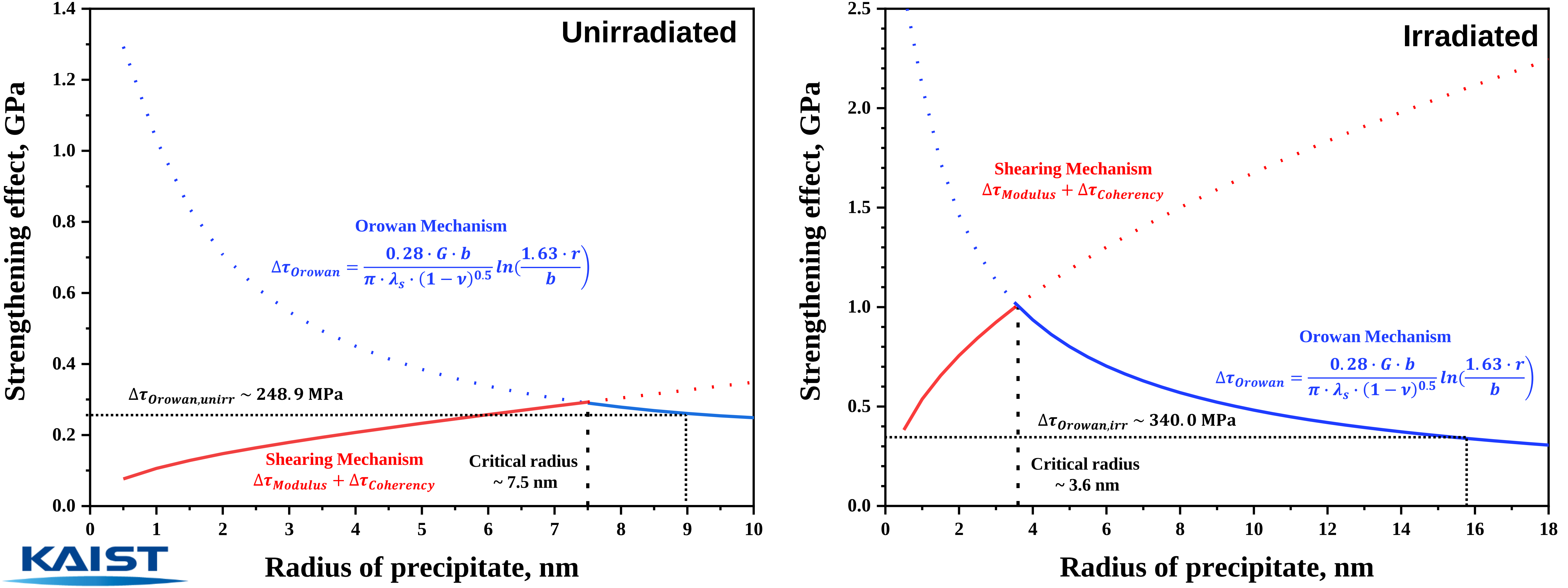

Results : Microstructural Evolution

TEM analysis on microstructural evolution of B2-NiAl

- **Coarsening of Fe-Cr rich phase in large B2-NiAl (Further Analyses Required)**
  - **Before Irradiation**
    - Fine Fe-Cr rich precipitates inside large B2-NiAl precipitates
    - Average size : 15.71 ± 4.98 nm (Considering only more than 10 nm size)
  - **After Irradiation**
    - Coarsening of Fe-Cr rich precipitates inside large B2-NiAl precipitates
    - Average size : 34.57 ± 7.69 nm (Considering only more than 10 nm size)
    - **More distinct Fe & Cr distribution** within large B2 → **Distinct phase separation within B2-NiAl precipitates**

Unirradiated ADSS (Ferritic matrix)

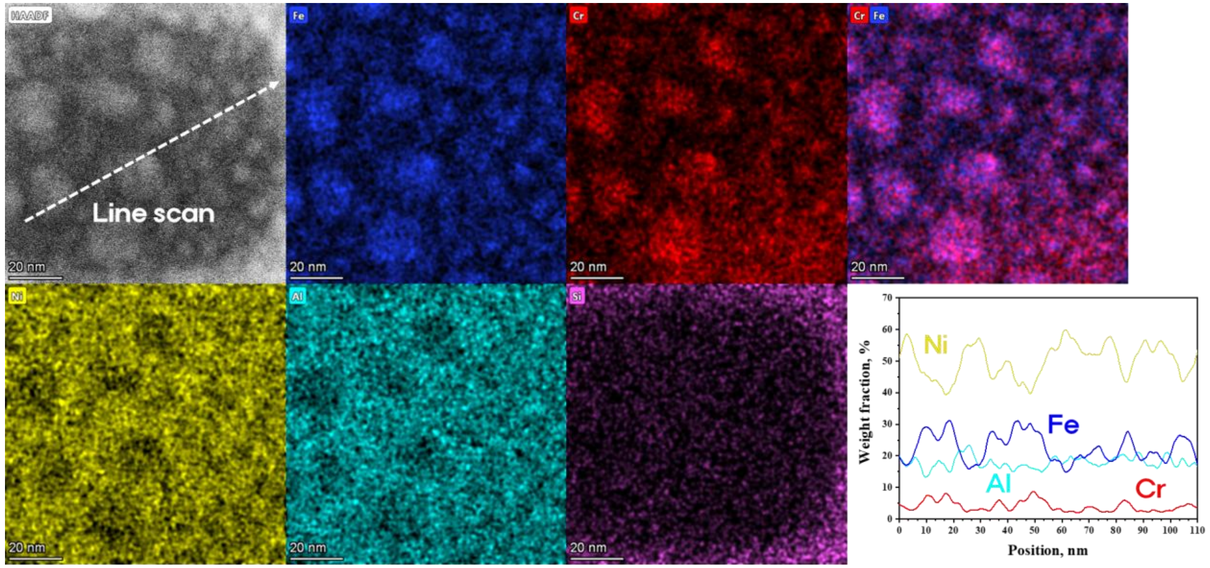

Irradiated ADSS (Ferritic matrix)

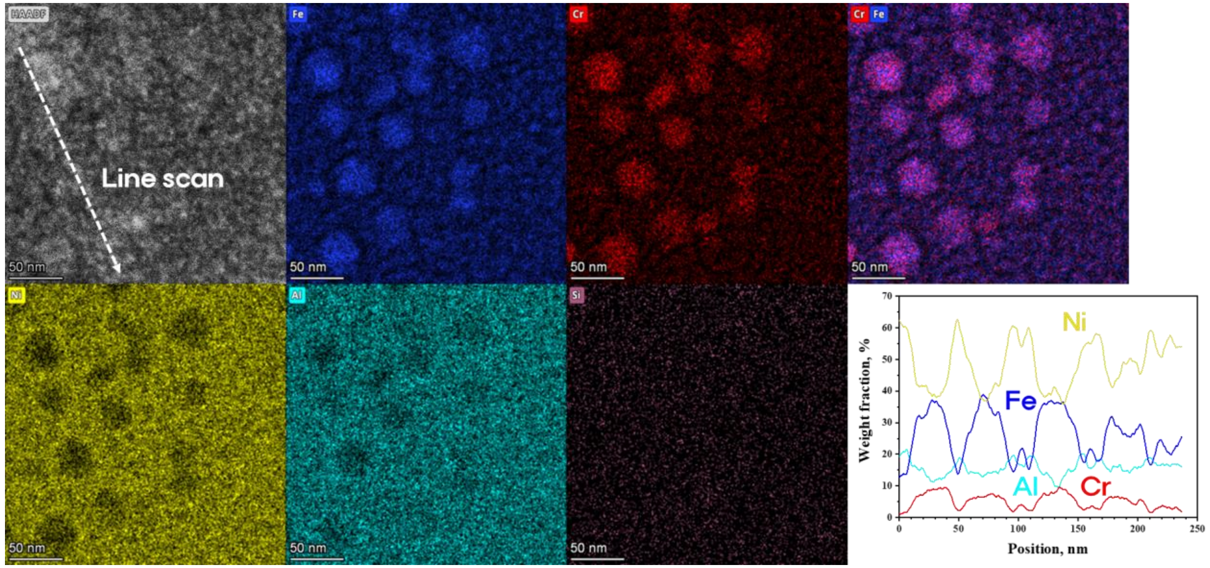

Results : Evaluation of Nano-hardness

❑ Correlation between Strengthening Mechanism & Nano-hardness Measurement

- **Microstructural Evolution vs. Nano-hardness Measurement after proton irradiation**
  - **Austenitic matrix**
    - ☐ Dissolution of B2-NiAl (Softening)
    - ☐ Formation of γ'-Ni_3Al (Hardening)

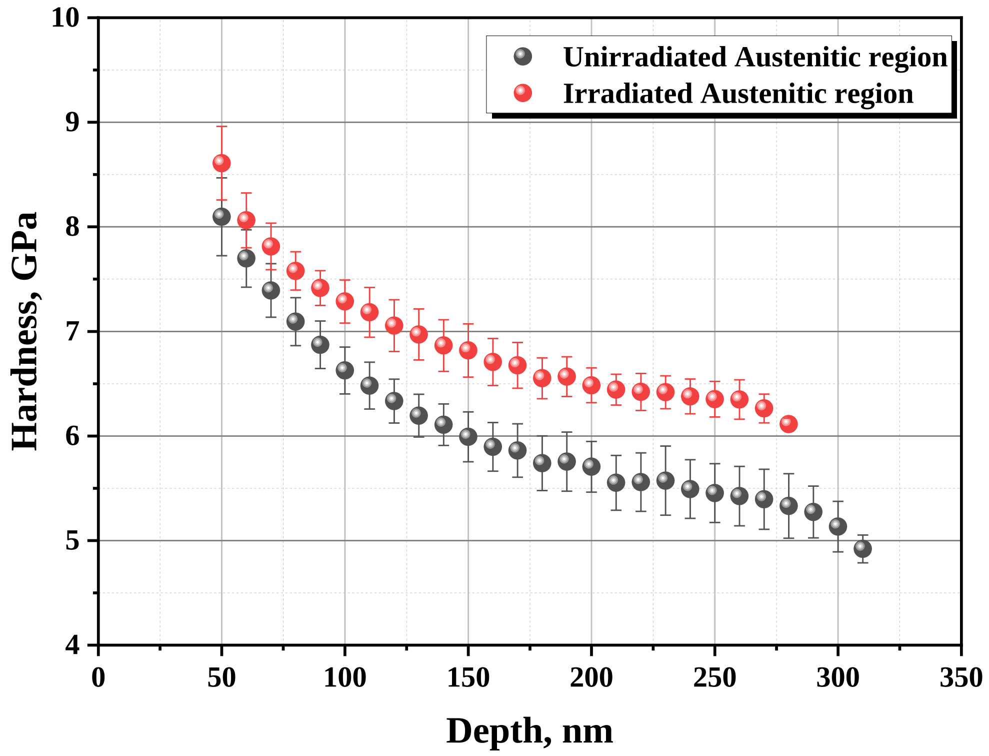

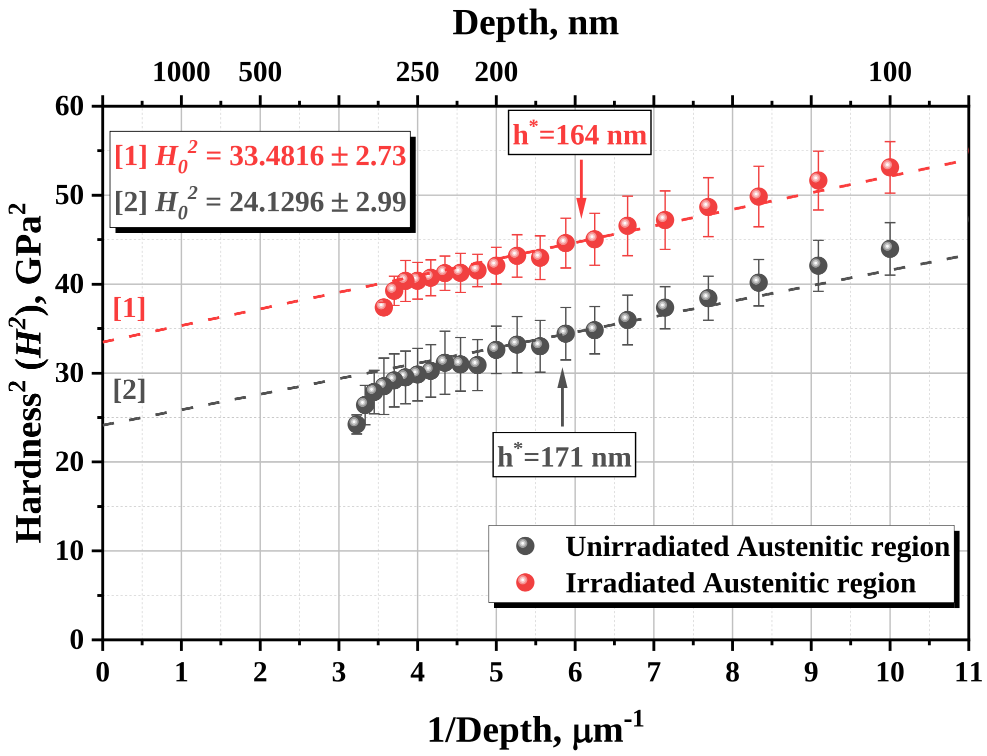

Results : Evaluation of Nano-hardness

❑ Correlation between Strengthening Mechanism & Nano-hardness Measurement

- **Microstructural Evolution vs. Nano-hardness Measurement after proton irradiation**
  - **Ferritic matrix (5.61±0.23 → 5.91±0.27 GPa)**
    - ◻ Dissolution of B2-NiAl (Softening) + Re-precipitation of B2-NiAl (Hardening)
    - ◻ Coarsening of nano-sized B2-NiAl (Hardening)
    - ◻ **Coarsening of Fe-Cr rich precipitates inside large B2-NiAl**

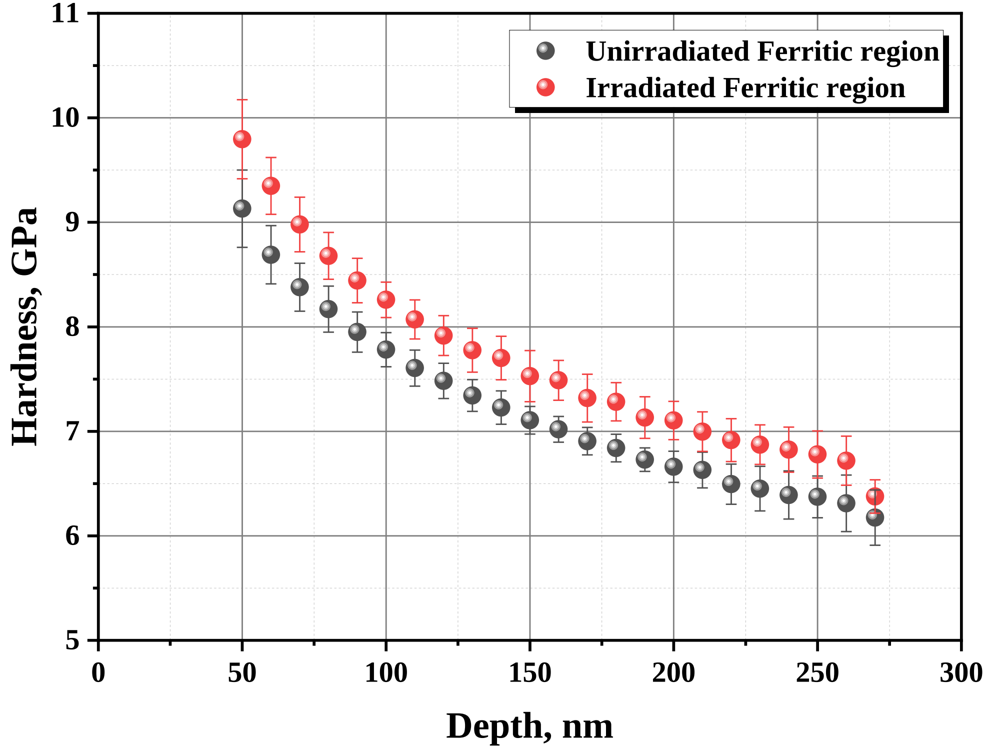

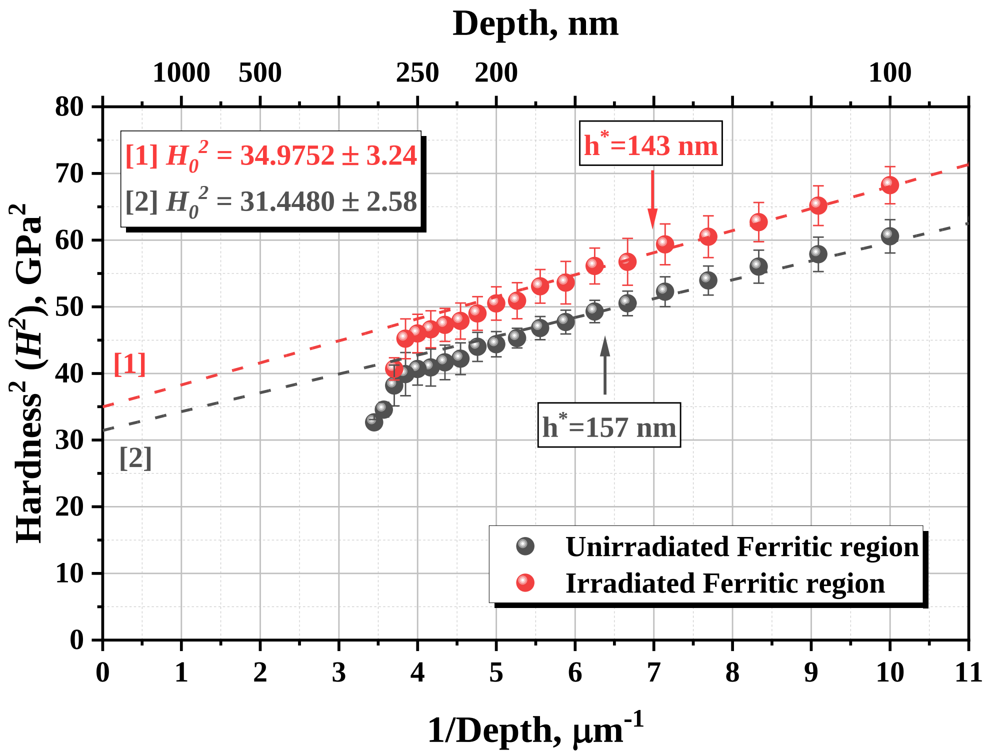

Results : Evaluation of Nano-hardness

Correlation between Strengthening Mechanism & Nano-hardness Measurement

- **Microstructural Evolution vs. Nano-hardness Measurement after proton irradiation**
  - **Hardness Convergence after the proton irradiation**
    - The formation of γ'-Ni_3Al precipitates sharply increases the bulk-hardness of austenitic matrix **(4.91±0.3 → 5.78±0.24 GPa)**
    - The combination of softening & hardening effect causes smaller increase in bulk-hardness of ferritic matrix **(5.61±0.23 → 5.91±0.27 GPa)**
    - The bulk-hardness difference between austenitic & ferritic matrix decreases

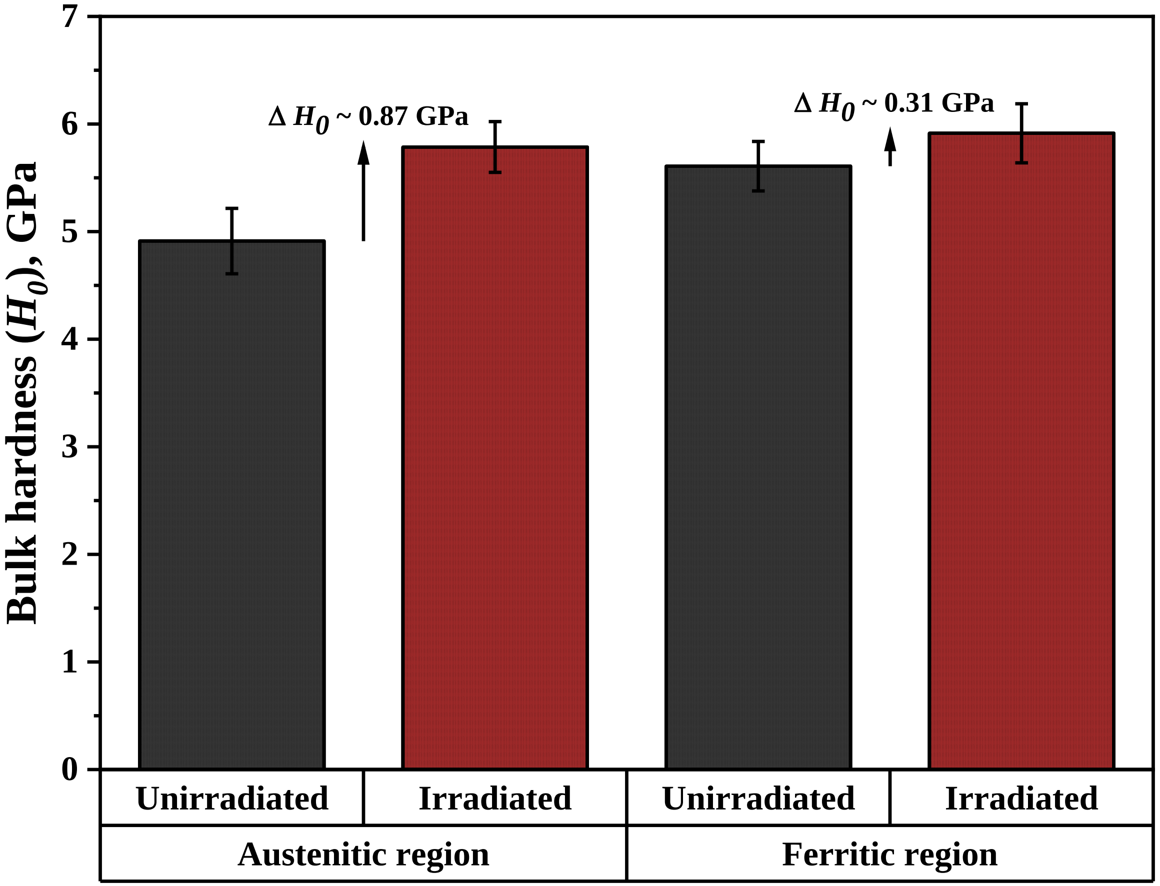

Different microstructural evolutions in austenitic & ferritic matrix lead to convergence in mechanical property under proton irradiation

Summary & Conclusion

❑ Correlation between Microstructural Evolution and Nano-mechanical Properties

- **Proton irradiation based on SRIM Simulation**
  - **Test condition**
    - ◻ 2 MeV proton beam at 360 ℃
    - ◻ Target damage : 1 ~ 2 dpa near 1 μm depth region

- **Microstructural Evolution vs. Nano-hardness Measurement after proton irradiation**
  - **Austenitic matrix**
    - ◻ Substantial hardening (+ 0.87 GPa)
    - ◻ Mainly due to the formation of nano-sized γ'-Ni_3Al precipitates (compared to the dissolution of large B2-NiAl precipitates)
  - **Ferritic matrix**
    - ◻ Smaller hardening (+0.31 GPA)
    - ◻ Balancing between softening (Dissolution of B2-NiAl) and hardening (Coarsening of nano-sized B2 and re-precipitation of B2-NiAl)
    - ◻ Effect of coarsening and loss of coherency in Fe-Cr rich precipitates on radiation hardening requires further microstructural & nano-indentation based analyses
  - **Convergence in mechanical property under proton irradiation condition**
    - ◻ Different microstructural evolutions in both matrices lead to the decrease in bulk-hardness difference

Energy for Earth !!

Thank you!